JOURNAL OF THEORETICAL AND APPLIED MECHANICS
51, 2, pp. 375-385, Warsaw 2013

NUMERICAL TESTING OF FLIGHT STABILITY OF SPIN-STABILIZED ARTILLERY PROJECTILES

Leszek Baranowski
Military University of Technology, Faculty of Mechatronics and Aerospace, Warsaw, Poland
e-mail: leszek.baranowski@wat.edu.pl

The paper presents results of numerical research on the effect of the twist rate, muzzle velocity, Magnus moment and firing disturbances (cross and range wind) on the stability of flight of a Denel 155 mm artillery projectile (Assegai M2000 Series) for flat and steep trajectories.

Key words: spin-stabilized projectile, flight stability, Magnus moment

1. Introduction

Analytical solutions of equations of motion of spin-stabilized artillery projectiles obtained under certain simplifying assumptions (small total angle of attack α_t and fixed factors in linearized differential equations of motion) identify essential conditions for stabilizing projectiles on the whole trajectory (Dmitrievskij, 1979; Gacek, 1998; Shapiro, 1956)
— for the initial (near-straight-line) part of the trajectory, it is required that

$$\sigma = 1 - \frac{b}{a^2} > 0 \tag{1.1}$$

where a is the precession velocity

$$a = \frac{I_x p_0}{2I_y} \qquad b = \frac{M_\alpha^A}{I_y} = \frac{C_{m\alpha}^A \rho V^2 S d}{2I_y}$$

— then, for the curvilinear section of the trajectory, it is required that the angle δ_r contained between the vector of velocity of the projectile and the dynamic balance axis is small enough not to cause overturning (tumbling) of the projectile near the trajectory apex

$$\delta_r = \frac{2a}{b}\frac{g\cos\gamma}{V} = \frac{2I_x p_0 g\cos\gamma}{\rho V^3 S d C_{m\alpha}^A} \tag{1.2}$$

English-language literature (McCoy, 1999; PRODAS v3 User manual; Textbook of Ballistics and Gunnery, 1987) proposes the following equation for "gyroscopic stability factor" based on linearized equations of motion of the projectile as a rigid body

$$S_g = \frac{2I_x^2 p^2}{\pi\rho I_y d^3 V^2 C_{M_\alpha}} \tag{1.3}$$

The condition for stable projectile flight in the initial section of the trajectory is as follows

$$S_g > 1 \tag{1.4}$$

The paper attempts to take a look at the problem of stability of flight of artillery projectile on the whole flight trajectory based on a non-linear mathematical model of motion of the projectile as a rigid body presented in the earlier Author's work (2011).

For this purpose, a computer application was developed for simulating the firing of the test projectile from Howitzer-gun "Krab" using the aforementioned mathematical model. Denel 155mm artillery projectile (Assegai M2000 Series) was used as the test projectile. The computer application was used to carry out all-inclusive tests of flight stability of the projectile fired with different muzzle velocities from a 52 caliber barrel to determine the twist rate and quadrant elevation range optimal from the point of view of projectile flight stability. The paper presents selected results of analysis of firing with extreme charges (minimum velocity $V_{K0} = 319\,\mathrm{m/s}$ for the 1st charge and the maximum velocity $V_{K0} = 935\,\mathrm{m/s}$ for the 6th charge) designed to reveal the following:

- the effect of the twist rate in the end of the barrel expressed in calibers η on the stability of flight of the projectile fired at a small and at the maximum quadrant elevation QE;
- the effect of muzzle velocity on dynamic properties of the projectile fired at a small QE (flat trajectory) and the maximum QE (steep trajectory);
- the effect of firing disturbances on the behavior of the projectile on the trajectory.

2. Characteristics of the physical model of the test projectile

The development of the flight simulation computer program of artillery projectiles requires determination of the so-called physical model (Dziopa *et al.*, 2010; Koruba *et al.*, 2010; Kowaleczko and Żyluk, 2009; Ładyżyńska-Kozdraś, 2012), which includes the following characteristics:

a) Structure characteristics:
   - geometries
   - mass and inertia
   - elasticity

b) Aerodynamic characteristics.

c) Surrounding environment:
   - density, viscosity, temperature, pressure, velocity and wind direction depending on weather, flight altitude, etc. The simulation adopted the International Standard Atmosphere (ISO 2533, 1975) as the reference.

Because of compact design and high rigidity of artillery projectiles, the frequency of proper vibration of elastic components of the deliberated test projectile is many times higher than the frequency of its oscillation around the center of mass, which enables treating the test projectile as a non-deformable solid body with 6 degrees of freedom.

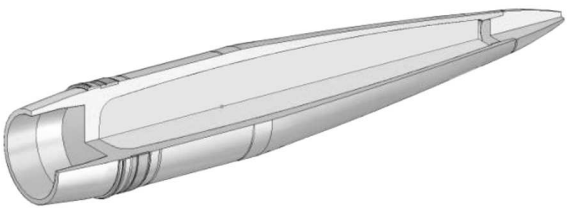

Fig. 1. Overview: test projectile solid model

In line with the prevailing trend, the theoretical calculation of the mass and inertia characteristics of the test projectile used the SolidWorks software package from SolidWorks Corporation (one of popular CAD/CAM suites). The computation of the characteristics assumes that the projectile is an axial-symmetric solid with symmetric mass and inertia. See Fig. 1 for an overview

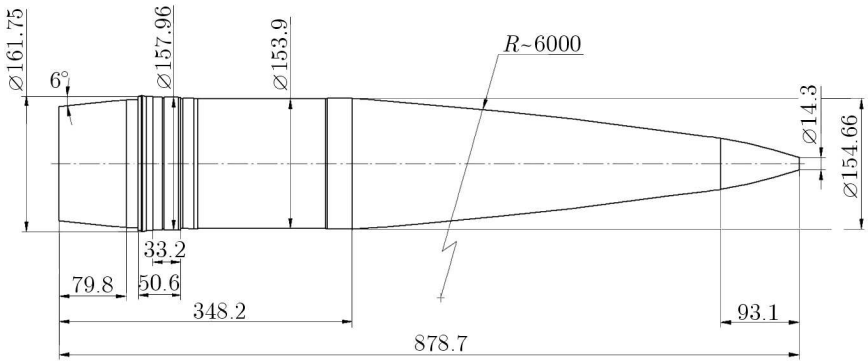

Fig. 2. Main dimensions of the test projectile

of the test projectile (solid model) and Fig. 2 for the main dimensions used for the computation of geometric and aerodynamic characteristics.

The mass and inertia characteristics of the test projectile computed using the SolidWorks software are as follows:

— mass: $m = 43.7\,\mathrm{kg}$

— coordinate of position of the center of projectile mass relative to the nose (Fig. 2): $x_{CG} = 0.563\,\mathrm{m}$

— moments of inertia of the projectile I_x, I_y, I_z in the body-fixed system $0xyz$: $I_x = 0.1444\,\mathrm{kgm}^2$, $I_y = 1.7323\,\mathrm{kgm}^2$, $I_z = 1.7323\,\mathrm{kgm}^2$.

Aerodynamic characteristics of the test projectile were determined using an off-shelf software application: Arrow Tech PRODAS 3.5.3 dedicated to computer-aided designing weaponry. See Tables 1 and 2 for the results of computation of aerodynamic characteristics as a function of the Mach number M for: $p^* = pd/(2V)$, $q^* = qd/(2V)$, $r^* = rd/(2V)$ and $S = \pi d^2/4$.

Table 1. Aerodynamic characteristics of the test projectile as a function of the Mach number

M [–]	$C^A_{X_0}$ [–]	$C^A_{X_{\alpha^2}}$ [rad$^-$2]	$C^A_{Z\alpha}$ [rad$^-$1]	$C^A_{Yp\alpha}$ [rad$^-$1]	C^A_{lp} [–]	$C^A_{m\alpha}$ [rad$^-$1]	C^A_{mq} [–]
0.010	0.144	1.90	1.624	−0.85	−0.0308	3.755	−9.5
0.400	0.144	1.90	1.623	−0.85	−0.0308	3.784	−9.2
0.600	0.144	1.91	1.629	−0.85	−0.0308	3.774	−9.5
0.700	0.144	2.10	1.633	−0.86	−0.0308	3.763	−9.8
0.800	0.146	2.21	1.638	−0.87	−0.0308	3.785	−10.3
0.900	0.160	2.30	1.655	−0.88	−0.0308	3.843	−11.0
0.950	0.202	2.50	1.661	−0.91	−0.0309	3.825	−11.9
0.975	0.240	2.64	1.694	−0.93	−0.0308	3.736	−12.8
1.000	0.284	2.74	1.746	−0.95	−0.0306	3.577	−14.0
1.025	0.313	2.89	1.823	−1.06	−0.0301	3.570	−15.2
1.050	0.332	3.09	1.902	−1.20	−0.0296	3.558	−16.8
1.100	0.337	3.30	1.962	−1.07	−0.0293	3.601	−18.8
1.200	0.340	3.51	2.006	−0.99	−0.0290	3.675	−20.8
1.500	0.321	3.87	2.128	−0.92	−0.0291	4.014	−22.6
2.000	0.276	4.36	2.209	−0.86	−0.0297	3.774	−22.8
2.500	0.240	4.86	2.299	−0.78	−0.0302	3.583	−24.3
3.000	0.214	4.37	2.359	−0.70	−0.0299	3.460	−25.6

Table 2. Derivative of the Magnus moment coefficient for the test projectile as a function of the total angle of attack α_t and the Mach number

C_{np}^{A} [–]							
M	α_t [deg]						
[–]	0	1	2	3	5	10	20
0.010	0	−0.0069	−0.0002	0.0286	0.1316	0.3313	0.6349
0.400	0	−0.0069	−0.0002	0.0286	0.1316	0.3313	0.6349
0.600	0	−0.0069	−0.0002	0.0286	0.1316	0.3313	0.6349
0.700	0	−0.0091	−0.0047	0.0227	0.1348	0.3353	0.6425
0.800	0	−0.0144	−0.0137	0.0120	0.1229	0.2971	0.5670
0.900	0	−0.0054	−0.0002	0.0223	0.1028	0.2519	0.4764
0.950	0	0.0033	0.0144	0.0393	0.1340	0.3120	0.5892
0.975	0	0.0068	0.0194	0.0420	0.1174	0.2879	0.5447
1.000	0	0.0099	0.0243	0.0463	0.1124	0.2181	0.4089
1.025	0	0.0136	0.0304	0.0523	0.1084	0.2104	0.3945
1.050	0	0.0148	0.0317	0.0525	0.1062	0.2059	0.3865
1.100	0	0.0140	0.0296	0.0480	0.0909	0.1838	0.3443
1.200	0	0.0121	0.0257	0.0413	0.0723	0.1377	0.2553
1.500	0	0.0126	0.0251	0.0377	0.0640	0.1232	0.2289
2.000	0	0.0124	0.0247	0.0366	0.0609	0.1156	0.2154
2.500	0	0.0122	0.0241	0.0356	0.0605	0.1144	0.2131
3.000	0	0.0121	0.0240	0.0356	0.0605	0.1145	0.2133

3. Effect of the twist rate on stability of the projectile fired at small and large quadrant elevation

The effect of the twist rate in the end of the gun barrel η (expressed in calibers per revolution) and effect of the Magnus moment on stability of the projectile on the trajectory was checked by stimulating the firing with the minimum ($V_{K0} = 319\,\mathrm{m/s}$) and maximum ($V_{K0} = 935\,\mathrm{m/s}$) initial (muzzle) velocities and a flat trajectory ($QE = 10\,\mathrm{deg}$) and steep trajectory ($QE = 70\,\mathrm{deg}$) for four values of the twist rate $\eta = 15$, 20, 25, 30 calibers.

See Table 3 for the basic inputs to the simulation and corresponding factors that were used for evaluating stability in the initial section of the trajectory using equations (1.1) and (1.3).

Table 3. Main initial inputs to the firing simulation for testing of the twist rate η

Twist rate η	Charge 1 $V_{K0} = 319\,\mathrm{m/s}$				Charge 2 $V_{K0} = 935\,\mathrm{m/s}$			
[caliber]	p_0 [rad/s]	S_g [–]	σ [–]	$\sqrt{\sigma}$ [–]	p_0 [rad/s]	S_g [–]	σ [–]	$\sqrt{\sigma}$ [–]
15	862.0	3.2	0.69	0.83	2526.8	3.5	0.71	0.84
20	646.6	1.8	0.45	0.67	1895.1	1.96	0.49	0.7
25	517.3	1.15	0.13	0.36	1516.1	1.25	0.2	0.45
30	431.0	0.8	−0.25		1263.4	0.8	−0.15	

The initial (muzzle) value of the spin rate of the projectile was computed using the known dependence

$$p_0 = \frac{2\pi V_{K0}}{\eta d} \tag{3.1}$$

In addition, it was assumed at the muzzle that the total angle of attack $\alpha_t = 0$ and angular velocities of the projectile (in the plane perpendicular to the longitudinal axis of the projectile) depend on the quadrant elevation QE and initial velocity V_{K0} (see Table 4) but are independent of the twist rate η.

Table 4. Typical initial values of projectile angular velocities in the plane perpendicular to the longitudinal axis of the projectile (McCoy, 1999)

Quadrant elevation QE [deg]	Charge 1 $V_{K0} = 319$ m/s		Charge 2 $V_{K0} = 935$ m/s	
	q_0 [rad/s]	r_0 [rad/s]	q_0 [rad/s]	r_0 [rad/s]
10	1.235	0	4.000	0
70	1.270	0	4.015	0

Figures 3 and 4 show line diagrams of the total angle of attack $\alpha_t(t)$ (for different $\eta = 15$, 20, 25 and 30) in the simulation of a flat trajectory ($QE = 10$ deg) with the minimum and maximum initial velocities. In addition, the left side diagrams illustrate the effect of omitting the Magnus moment from the computation, while the right side one takes it into account.

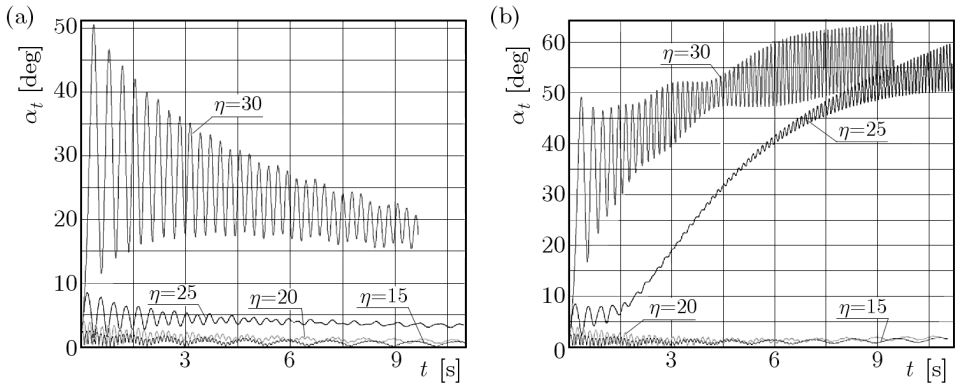

Fig. 3. Total angle of attack α_t versus time for different twist rates η, in the case of flat trajectories and the minimum initial velocity $V_{K0} = 319$ m/s; (a) without the Magnus moment, (b) with the Magnus moment

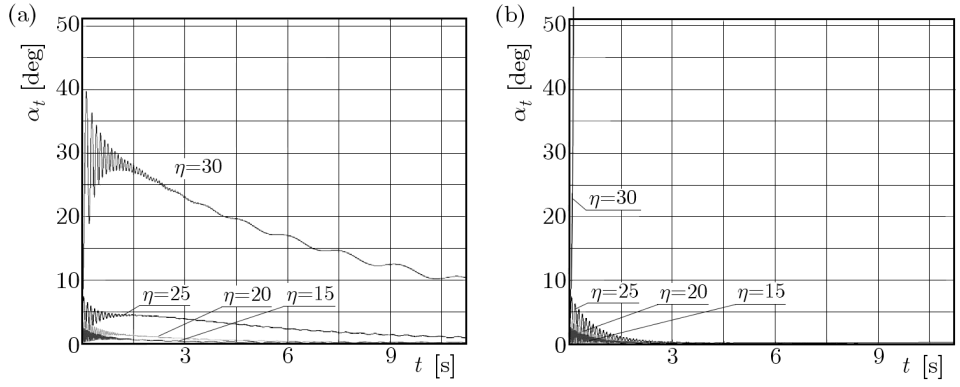

Fig. 4. Total angle of attack α_t versus time for different twist rates η, in the case of flat trajectories and the maximum initial velocity $V_{K0} = 935$ m/s; (a) without the Magnus moment, (b) with the Magnus moment

Likewise, Figs. 5 and 6 show line diagrams of the total angle of attack $\alpha_t(t)$ for a steep trajectory ($QE = 70$ deg) with the minimum and maximum initial velocities, with and without the Magnus moment.

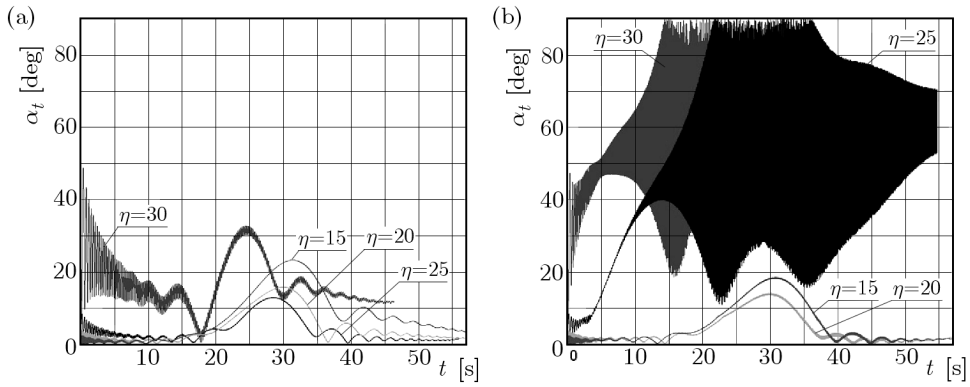

Fig. 5. Total angle of attack α_t versus time for different twist rates η, in the case of steep trajectories and the minimum initial velocity $V_{K0} = 319\,\mathrm{m/s}$; (a) without the Magnus moment, (b) with the Magnus moment

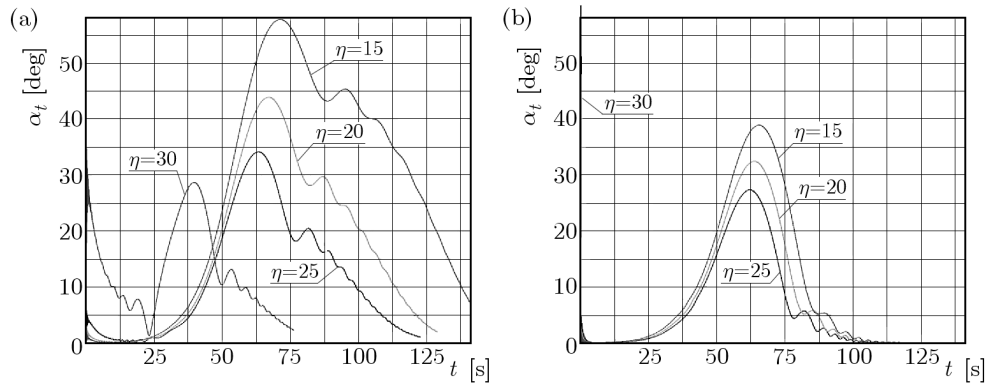

Fig. 6. Total angle of attack α_t versus time for different twist rates η, in the case of steep trajectories and the maximum initial velocity $V_{K0} = 935\,\mathrm{m/s}$; (a) without the Magnus moment, (b) with the Magnus moment

Initial numerical tests performed using the non-linear model of projectile motion confirmed, following the existing literature, a huge effect of the twist rate η on the details of projectile motion around the center of its mass both for small and the maximum quadrant elevation (see Figs. 3-4 and Figs. 5-6, respectively). For $\eta = 30$ calibers, the projectile is clearly unstable ($\sigma < 0$, $S_g < 1$), which is confirmed by $\alpha_t(t)$ lines in, basically, all diagrams, particularly if the Magnus moment is included in the computation (Figs. 3b, 4b, 5b and 6b).

The case of $\eta = 25$ calibers is peculiar because based on the criteria of stability ($\sigma > 0$, $S_g > 1$) the projectile should be stable while computations taking into account the Magnus moment for the minimum initial velocity (Figs. 3b and 5b) show that the projectile is dynamically unstable. The cause is a negative Magnus moment occurring at small total angle of attack and subsonic flight velocities (see Table 2).

Based on the analysis of flight stability of the test projectile, it was assumed for the purposes of further simulation tests that the twist rate in the end of the gun barrel η would be equal to 20 calibers.

4. Effect of muzzle velocity on the dynamic properties of the projectile fired at a small and large quadrant elevation

This test simulated the following parameters: twist rate $\eta = 20$ calibers, minimum muzzle velocity $V_{K0} = 319\,\mathrm{m/s}$, maximum muzzle velocity $V_{K0} = 935\,\mathrm{m/s}$, small quadrant elevation $QE = 10\,\mathrm{deg}$, large quadrant elevation $QE = 70\,\mathrm{deg}$, remaining initial conditions as in Tables 3

and 4. In order to determine the composite effect of the Magnus moment on the stability of flight of the projectile, the computations were made for two variants: with and without considering the Magnus moment.

Flight stability was evaluated based on the variation of the total angle of attack in time $\alpha_t(t)$ and the trace marked by the vertex of the projectile on the plane perpendicular to the vector of flight velocity in form of the function $\alpha_z = f(\alpha_y)$.

Illustrations of the angle α_y (projectile deviation from the vector of velocity in the horizontal plane) and angle α_z (projectile deviation from the vector of velocity in the vertical plane), defined as symmetrical, are shown in Fig. 7. The values of the angles were computed using the following equations

$$\alpha_y = \arctan\Big(-\frac{v_K - v_W}{u_K - u_W}\Big) \qquad \alpha_z = \arctan\Big(\frac{w_K - w_W}{u_K - u_W}\Big) \tag{4.1}$$

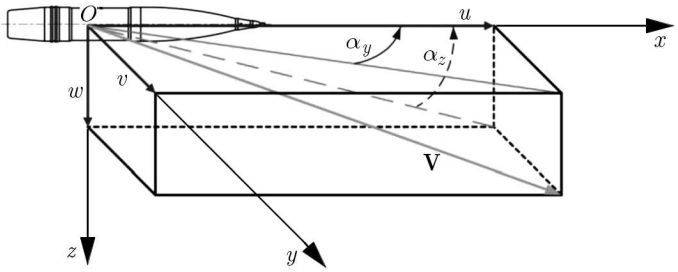

Fig. 7. Illustration of spatial positions of angles α_z and α_y (Baranowski, 2006)

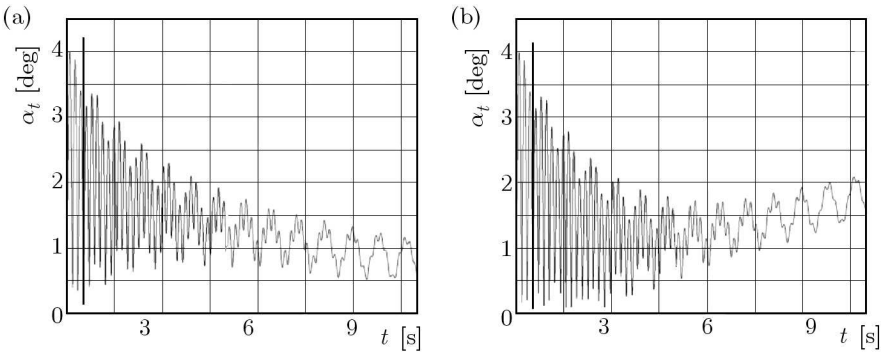

Fig. 8. Total angle of attack α_t versus time in the case of flat trajectories $QE = 10\,\text{deg}$ and the minimum initial velocity $V_{K0} = 319\,\text{m/s}$; (a) without the Magnus moment, (b) with the Magnus moment

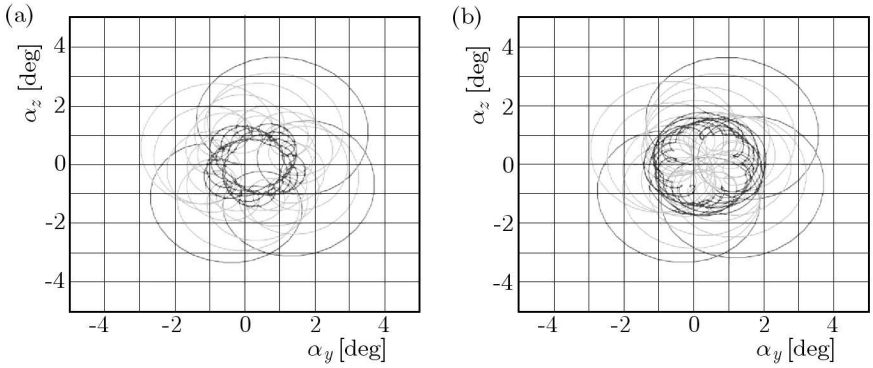

Fig. 9. Pitching and yawing motion in the case of flat trajectories QE=10 deg and the minimum initial velocity $V_{K0} = 319\,\text{m/s}$; (a) without the Magnus moment, (b) with the Magnus moment

Figures 8-11 show motion of the projectile around the center of its mass on a flat trajectory ($QE = 10\,\text{deg}$) for 11 initial seconds of flight. To make the diagrams clearer, three flight phases with related projectile motion parameters (total angle of attack α_t versus time and the trace marked by the vertex of the projectile illustrating pitching and yawing motion in form of the function $\alpha_z = f(\alpha_y)$) were distinguished with gray scale. In addition, the left side diagrams omit, and the right side one take into account, the Magnus moment.

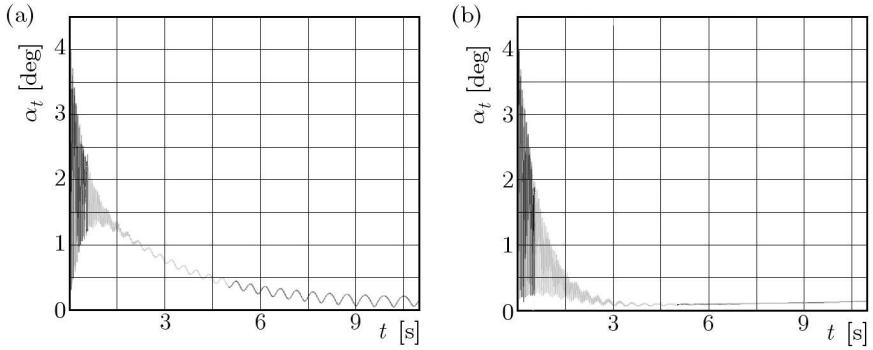

Fig. 10. Total angle of attack α_t versus time in the case of flat trajectories $QE = 10\,\text{deg}$ and the maximum initial velocity $V_{K0} = 935\,\text{m/s}$; (a) without the Magnus moment, (b) with the Magnus moment

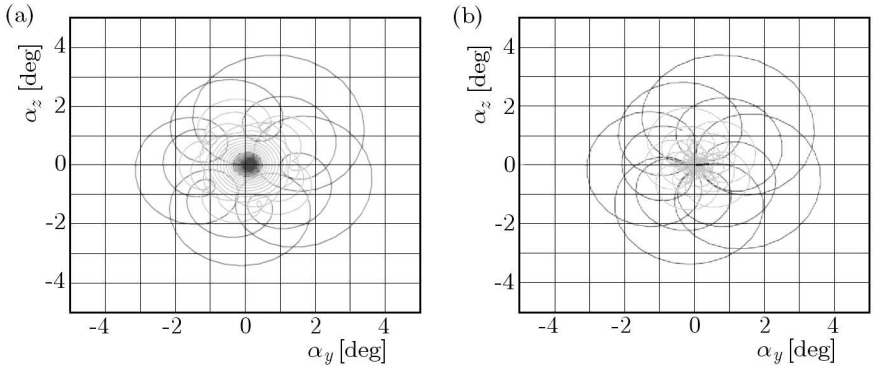

Fig. 11. Pitching and yawing motion in the case of flat trajectories $QE = 10\,\text{deg}$ and the maximum initial velocity $V_{K0} = 935\,\text{m/s}$; (a) without the Magnus moment, (b) with the Magnus moment

Likewise, as for the flat trajectory, Figs. 12-15 show the results of testing the effect of muzzle velocities (min. and max.) on the dynamic properties of the projectile flying along the steep trajectory, fired at a large quadrant elevation $QE = 70\,\text{deg}$.

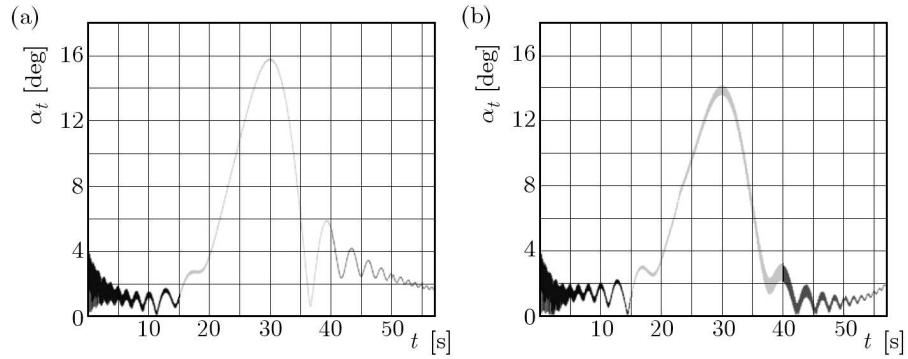

Fig. 12. Total angle of attack α_t versus time in the case of steep trajectories $QE = 70\,\text{deg}$ and the minimum initial velocity $V_{K0} = 319\,\text{m/s}$; (a) without the Magnus moment, (b) with the Magnus moment

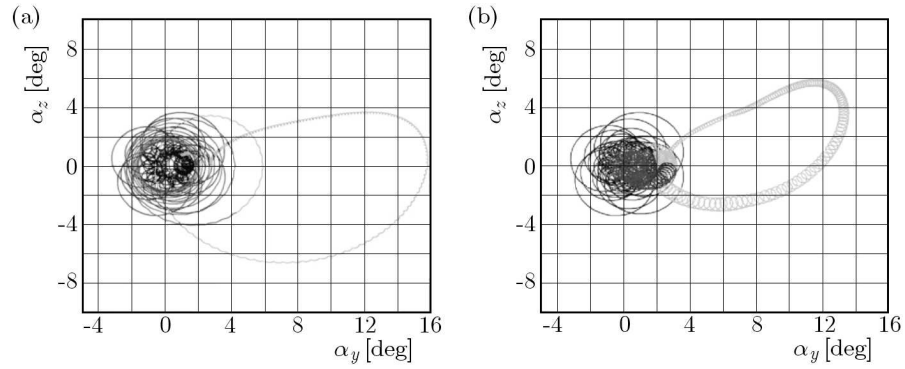

Fig. 13. Pitching and yawing motion in the case of steep trajectories $QE = 70\,\text{deg}$ and the minimum initial velocity $V_{K0} = 319\,\text{m/s}$; (a) without the Magnus moment, (b) with the Magnus moment

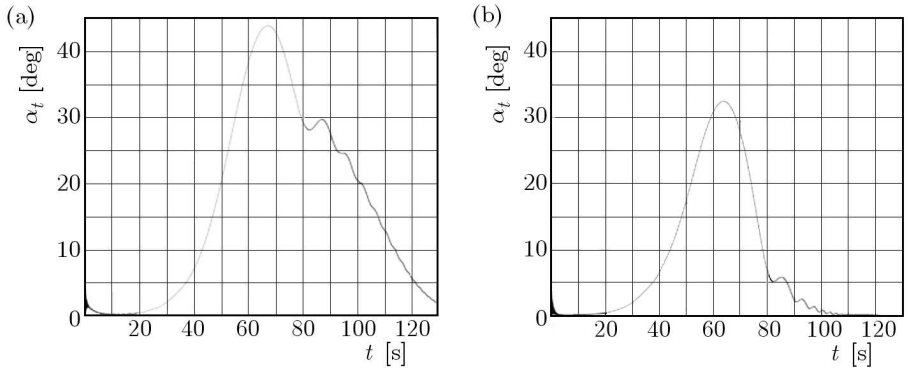

Fig. 14. Total angle of attack α_t versus time in the case of steep trajectories $QE = 70\,\text{deg}$ and the maximum initial velocity $V_{K0} = 935\,\text{m/s}$; (a) without the Magnus moment, (b) with the Magnus moment

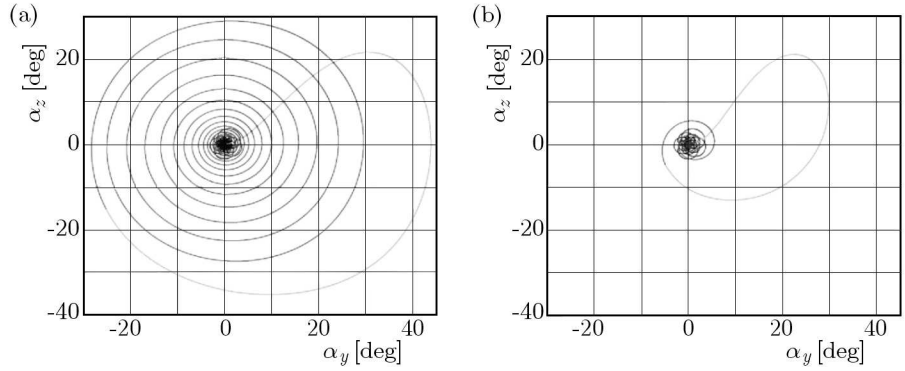

Fig. 15. Pitching and yawing motion in the case of steep trajectories $QE = 70\,\text{deg}$ and the maximum initial velocity $V_{K0} = 935\,\text{m/s}$; (a) without the Magnus moment, (b) with the Magnus moment

5. Results of tests of projectile behavior on the trajectory during firing in non-standard conditions

This point discusses the effect of perturbation of meteorological conditions on the flight dynamics of the spinning projectile, including specifically the effect of cross and range wind.

The following Figs. 16 and 17 show illustrative diagrams of selected parameters of flight of the test projectile flying flat trajectory ($QE = 10\,\text{deg}$) in calm conditions ($v_{W_g} = 0\,\text{m/s}$) and in conditions of strong cross wind blowing from: left side – $v_{W_g} = 20\,\text{m/s}$ and right side – $v_{W_g} = -20\,\text{m/s}$ since second second of the projectile flight.

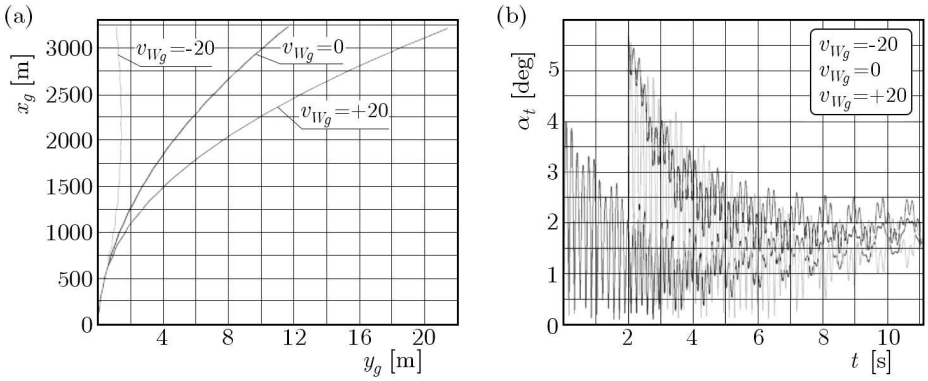

Fig. 16. (a) Effect of cross wind on the trajectory in the horizontal plane, (b) disturbing effect of cross wind on the total angle of attack α_t

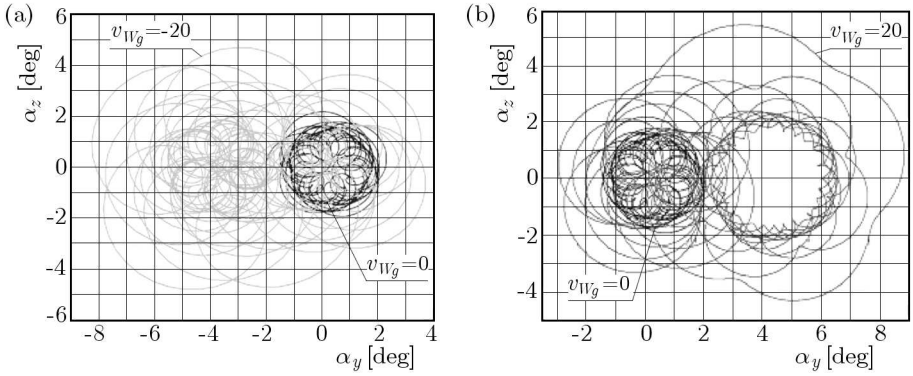

Fig. 17. Pitching and yawing motion for: (a) $v_{W_g} = -20\,\mathrm{m/s}$, (b) $v_{W_g} = +20\,\mathrm{m/s}$

6. Summary and conclusions

Results of testing flight stability in standard (undisturbed) conditions suggest the following:

- In general, the Magnus moment accelerates the suppression of the total angle of attack but, because it is negative for subsonic flight velocities, for the minimum initial velocity $V_{K0} = 319\,\mathrm{m/s}$ the growth of the total angle of attack destabilizes the projectile in the final flight phase (Fig. 8b and Fig. 12b).
- For flat trajectories, the maximum total angle of attack occurs at the start of the trajectory, whereas for steep trajectories near the vertex.
- For a large quadrant elevation, the details of projectile motion near the trajectory vertex (Fig. 13 and Fig. 15) are different than those provided by analytical solutions using the simplified model (Dmitrievskij, 1979; Gacek, 1998; Shapiro, 1956).
- Similarly, verifying the classical criteria of stability is not sufficient for selecting the twist rate of rifling: additional simulations are required taking into account the Magnus moment.

The results of numerical simulations of non-standard conditions confirmed, among others, the known phenomenon of projectile trajectory deflection in the direction of wind (Fig. 16a), but showed also clear difference of left- and right-sided wind on the projectile motion around the center of mass (see Figs. 16b and 17). This interesting phenomenon requires further theoretical and empirical testing.

Acknowledgement

The research work was supported by the Polish Ministry of Science and Higher Education in the years 2010-2013 within the framework of grant 423/B0/A.

References

1. Baranowski L., 2006, A mathematical model of flight dynamics of field artillery guided projectiles, *6th International Conference on Weaponry "Scientific Aspects of Weaponry"*, Waplewo, 44-53 [in Polish]
2. Baranowski L., 2011, *Modeling, Identification and Numerical Study of the Flight Dynamics of Ballistic Objects for the Need of Field Artillery Fire Control Systems*, Military University of Technology, Warsaw, p. 258 [in Polish]
3. Dmitrievskij A.A., 1979, *External Ballistics*, Mashinostroenie, Moscow [in Russian]
4. Dziopa Z., Krzysztofik I., Koruba Z., 2010, An analysis of the dynamics of a launcher-missile on a moveable base, *Bulletin of the Polish Academy of Sciences – Technical Sciences*, **58**, 4, 645-650
5. Gacek J., 1998, *Exterior Ballistics. Part II. Analysis of Dynamic Properties of Objects in Flight*, Military University of Technology, Warsaw, p. 316 [in Polish]
6. Koruba Z., Dziopa Z., Krzysztofik I., 2010, Dynamics and control of a gyroscope-stabilized platform in a self-propelled anti-aircraft system, *Journal of Theoretical and Applied Mechanics*, **48**, 1, 5-26
7. Kowaleczko G., Żyluk A., 2009, Influence of atmospheric turbulence on bomb release, *Journal of Theoretical and Applied Mechanics*, **47**, 1, 69-90
8. Ładyżyńska-Kozdraś E., 2012, Modeling and numerical simulation of unmanned aircraft vehicle restricted by non-holonomic constraints, *Journal of Theoretical and Applied Mechanics*, **50**, 1, 251-268
9. McCoy R.L., 1999, *Modern Exterior Ballistics. The Launch and Flight Dynamics of Symmetric Projectiles*, Schiffer Publishing
10. Shapiro J., 1956, *Exterior Ballistics*, MON, Warsaw [Polish translation]
11. PRODAS v3 User manual
12. *Textbook of Ballistics and Gunnery*, 1987, Her Majesty's Stationary Office, London
13. *The Modified Point Mass and Five Degrees of Freedom Trajectory Models*, 2009, STANAG 4355 Edition 3
14. *The ISO Standard Atmosphere*, 1975, ISO 2533

Badania numeryczne stabilności lotu klasycznego pocisku artyleryjskiego stabilizowanego obrotowo

Streszczenie

W pracy przedstawiono wyniki badań numerycznych wpływu długości skoku gwintu lufy, prędkości początkowej pocisku, momentu Magnusa oraz zakłóceń warunków strzelania (wiatru podłużnego i bocznego) na stabilność lotu 155 mm pocisku artyleryjskiego firmy Denel (Assegai M2000 Series) dla przypadku płaskiego i stromego toru lotu.

Manuscript received May 8, 2012; accepted for print July 2, 2012